Science
AAAS

Supplementary Materials for

Transcriptomes and metabolism define mouse and human MAIT cell populations

Shilpi Chandra[1,2,†,*], Gabriel Ascui[1,2,3,†], Thomas Riffelmacher[1,2,4,†], Ashu Chawla[5], Ciro Ramírez-Suástegui[1,6], Viankail C. Castelan[1,2], Gregory Seumois[1,6], Hayley Simon[1,6], Mallory P. Murray[1,2], Goo-Young Seo[1,2], Ashmitaa L. R. Premlal[5], Benjamin Schmiedel[1,6], Greet Verstichel[1,6], Yingcong Li[1,2,7], Chia-Hao Lin[7], Jason Greenbaum[5], John Lamberti[8,9], Raghav Murthy[8,10], John Nigro[8], Hilde Cheroutre[1,6], Christian H. Ottensmeier[11], Stephen M. Hedrick[7,12], Li-Fan Lu[7,13,14], Pandurangan Vijayanand[1,6] and Mitchell Kronenberg[1,2,7,*]

This PDF file includes:

Supplementary Figures S1 to S10

Table S1 to S10

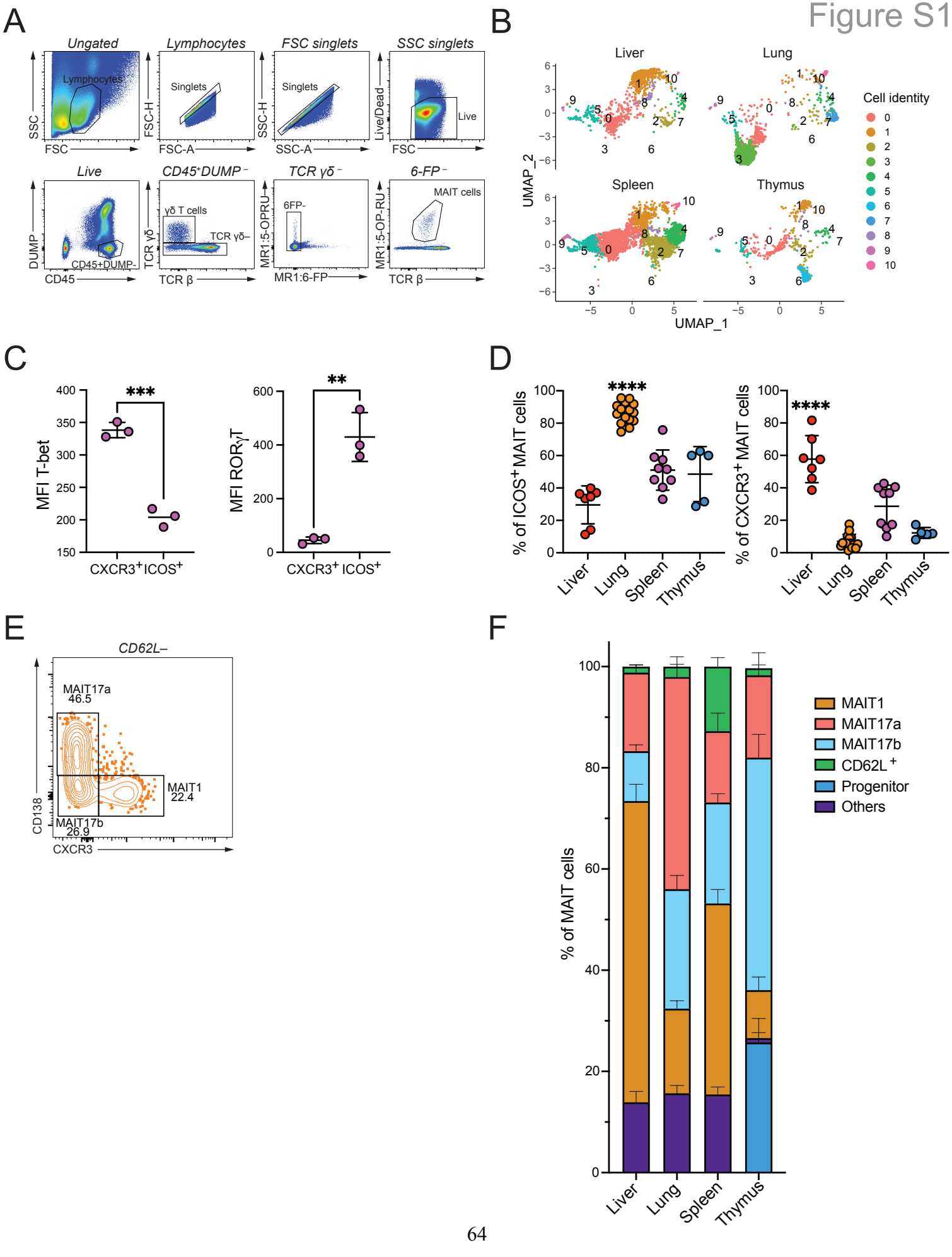
A
Ungated
Lymphocytes
FSC singlets
SSC singlets
SSC
FSC
FSC-H
FSC-A
SSC-H
SSC-A
Live/Dead
Singlets
Live
Live
CD45⁺DUMP⁻
TCR γδ⁻
6-FP⁻
DUMP
CD45
CD45+DUMP-
TCR γδ
TCR β
γδ T cells
TCR γδ−
MR1:5-OPRU
MR1:6-FP
6FP-
MR1:5-OP-RU
MAIT cells
B
Liver
Lung
Spleen
Thymus
UMAP_1
UMAP_2
Cell identity
C
MFI T-bet
MFI RORγT
CXCR3⁺ICOS⁺
D
% of ICOS⁺ MAIT cells
% of CXCR3⁺ MAIT cells
Liver
Lung
Spleen
Thymus
E
CD62L−
MAIT17a
46.5
MAIT1
22.4
MAIT17b
26.9
CD138
CXCR3
F
% of MAIT cells
MAIT1
MAIT17a
MAIT17b
CD62L⁺
Progenitor
Others

Figure S1: Characterization of mouse MAIT cell subsets

(A) Representative flow cytometry gating identified mouse lung MAIT cells, used for other tissues as well. Live/Dead Yellow negative single cell events were gated by excluding antigen-presenting cells (DUMP: CD11c, CD11b, IgD, B220) and γδ T cells from the $CD45^+$ population, $CD4^+$, $CD8^+$ double positive cells were excluded as well. The majority of experiments did not include a 6-FP loaded control, indicated when used. (B) UMAP plot showing the degree to which MAIT cell clusters are composed of cells from the indicated mouse tissues. Each cluster has the same UMAP coordinates as in Fig. 1A. (C) MFI indicating expression of T-bet and RORγT transcription factors in spleen MAIT cell subpopulations defined as $CXCR3^+$ and $ICOS^+$. Paired t-test. n = 3. *: $p < 0.05$; **: $p < 0.01$; (D) Frequency of $ICOS^+$ and $CXCR3^+$ MAIT cells in the indicated tissues. One-way ANOVA with post-hoc Tukey test. Liver n = 7, Lung n= 15, Spleen n= 9, Thymus n= 5. ****: adjusted $p < 0.0001$. (E) Lung MAIT cell subpopulations were detected by flow cytometry according to markers for MAIT cell clusters determined by scRNA-seq. The total MAIT cell gate was initially separated by CD62L expression. The CD62L negative gate was further divided into MAIT17a ($ICOS^+CD138^+CXCR3^-$), MAIT17b ($ICOS^+CD138^-CXCR3^-$) or MAIT1 ($ICOS^-CD138^-CXCR3^+$). (F) Percentage of each MAIT cell subpopulation, as defined above, in different tissues. Using the global gating strategy defined in (E) in combination with thymus-specific markers to detect immature MAIT cells ($CD44^-CD24^+CCR9^+LEF1^+SATB1^+$), the proportion of MAIT cell subpopulations was determined for each tissue combined from 11 female C57BL/6 mice (12.3±6.1 weeks-old). Data from 5 additional thymus tissues also were included.

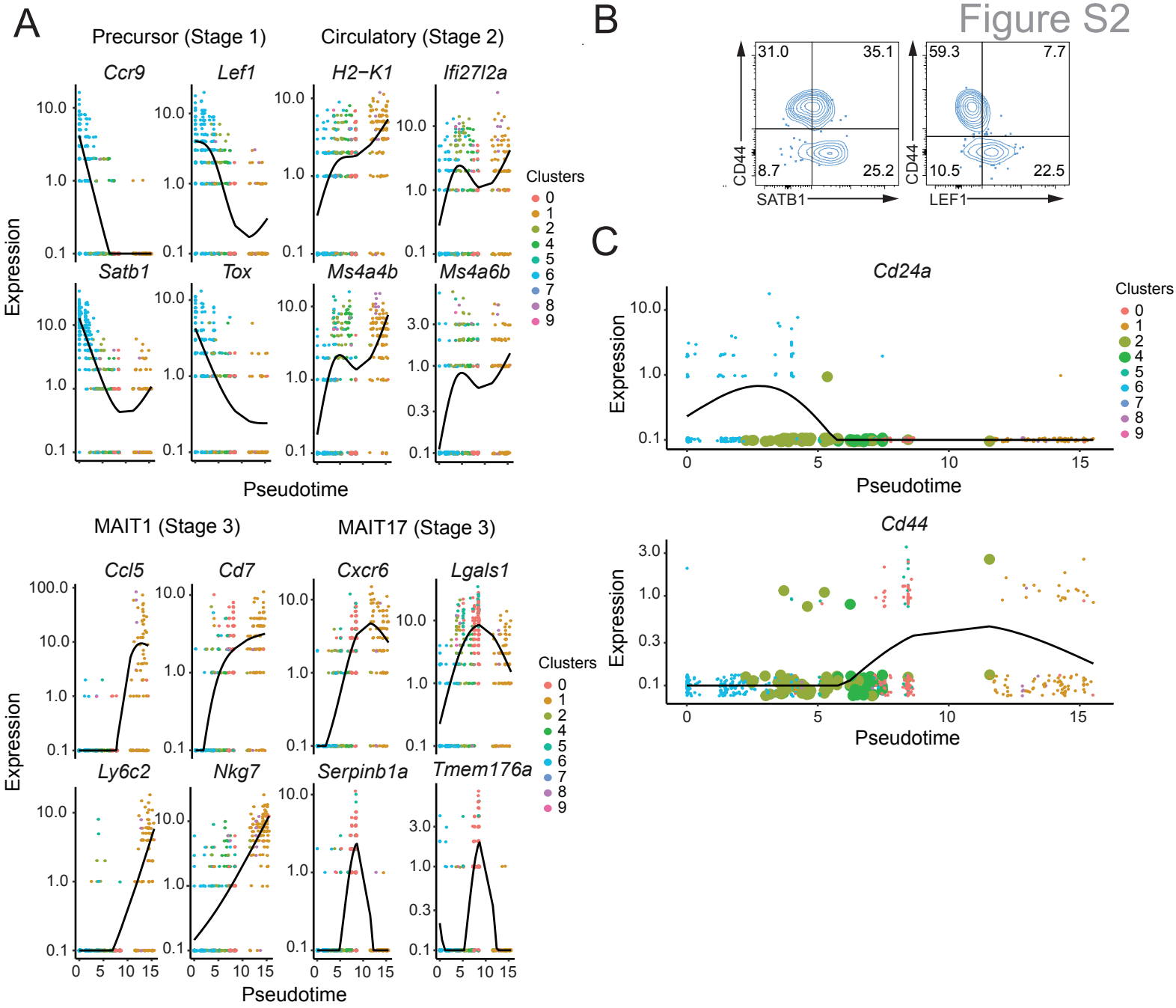
A
Precursor (Stage 1)
Circulatory (Stage 2)
Ccr9
Lef1
H2−K1
Ifi27l2a
Satb1
Tox
Ms4a4b
Ms4a6b
Expression
Pseudotime
Clusters
0
1
2
4
5
6
7
8
9
MAIT1 (Stage 3)
MAIT17 (Stage 3)
Ccl5
Cd7
Cxcr6
Lgals1
Ly6c2
Nkg7
Serpinb1a
Tmem176a
B
31.0
35.1
8.7
25.2
CD44
SATB1
59.3
7.7
10.5
22.5
LEF1
C
Cd24a
Cd44

Figure S2: Transcriptional signatures reveal different stages of thymus MAIT cell differentiation

(A) Expression of the indicated stage-specific genes along the pseudotime trajectory as constructed by Monocle 3. (B) Representative flow cytometry plots for staining of gated, thymus MAIT cells for surface expression of CD44 compared to intracellular SATB1 or LEF1, n = 5, from 2 experiments. (C) Expression of *Cd24a* and *Cd44* along the pseudotime trajectory for MAIT thymus cells as constructed by Monocle 3.

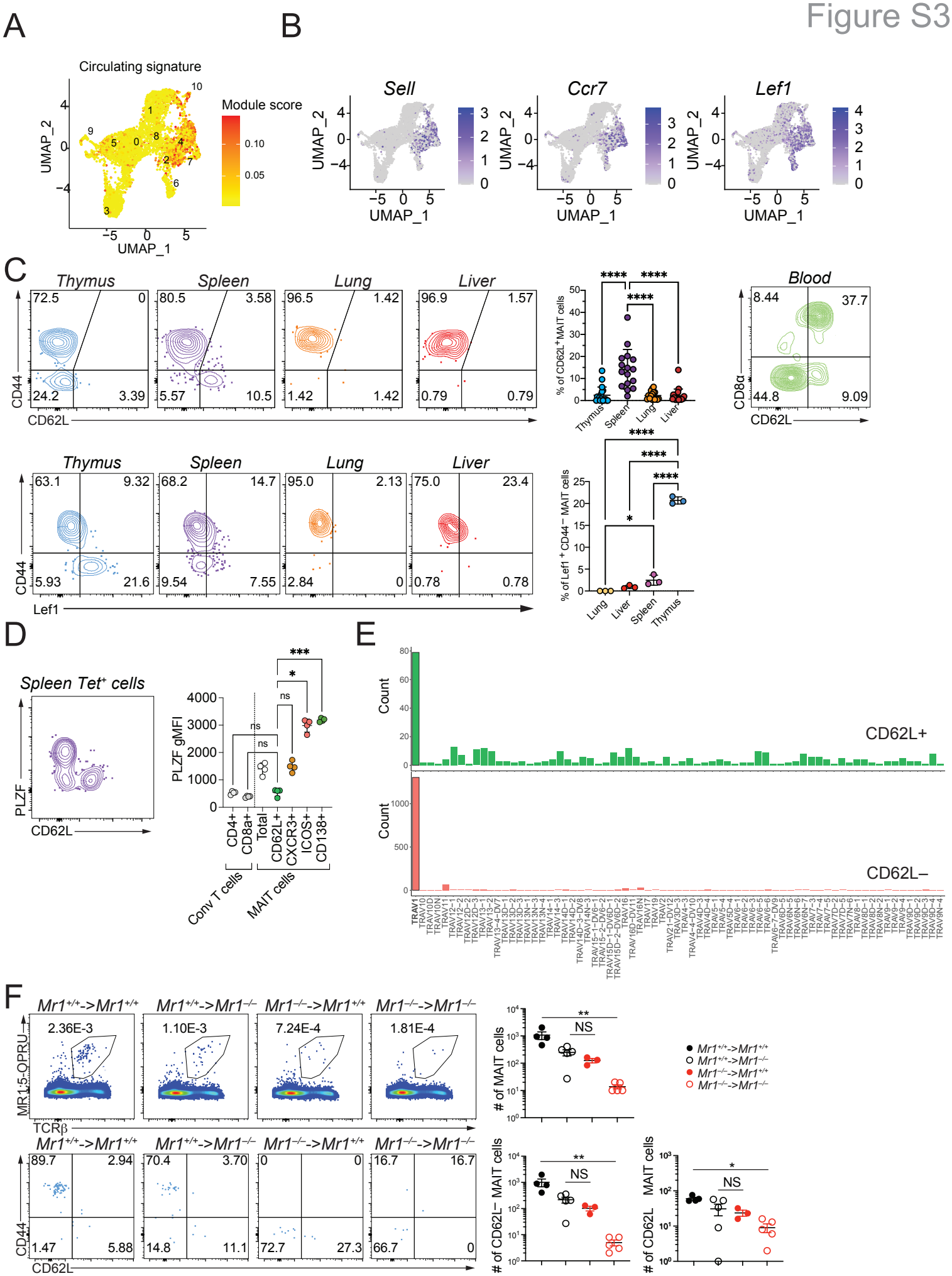
A
Circulating signature
Module score
0.10
0.05
UMAP_1
UMAP_2
B
Sell
Ccr7
Lef1
C
Thymus
Spleen
Lung
Liver
CD44
CD62L
Lef1
% of CD62L+ MAIT cells
% of Lef1+ CD44− MAIT cells
Blood
CD8α
D
Spleen Tet+ cells
PLZF
PLZF gMFI
Conv T cells
MAIT cells
E
Count
CD62L+
CD62L−
F
Mr1+/+->Mr1+/+
Mr1+/+->Mr1−/−
Mr1−/−->Mr1+/+
Mr1−/−->Mr1−/−
MR1:5-OPRU
TCRβ
# of MAIT cells
# of CD62L− MAIT cells
# of CD62L MAIT cells
NS

Figure S3: CD62L$^+$ mouse MAIT cell function and origin

(A) UMAP showing the circulatory gene expression signature scores from scRNA-seq data from mouse MAIT cells combined from liver, lung, spleen and thymus. (B) UMAP feature plots showing expression of key genes in MAIT cells combined from the four organs. (C) Representative plots showing CD44 and CD62L and Lef1 by MAIT cells from liver, lung, spleen and thymus. One-way ANOVA with post-hoc Tukey test. n = 4. ****: adjusted p-value < 0.0001. (D) Representative plot of CD62L and PLZF expressed by mouse spleen MAIT cells (top). Mean fluorescent intensity of PLZF expressed by mouse spleen CD4, CD8, and MAIT cell subsets. Paired one-way ANOVA with post-hoc Bonferroni test. n = 3. ***: adjusted p-value < 0.001, *: adjusted p-value < 0.05. (E) Number of cells expressing specific *Tcra* genes detected by scRNA-seq of sorted mouse CD62L$^+$ and CD62L$^-$ spleen MAIT cells. Representative of 2 experiments (Total of 1896 and 441 cells for CD62L$^-$ and CD62L$^+$ MAIT cells, respectively). (E) Mouse CD62L$^+$ and CD62L$^-$ spleen MAIT cells were isolated by cell sorting and cultured with anti-CD3/CD28 beads or stimulated with 5-OP-RU. *Left*: T-bet and RORγT expression were evaluated by flow cytometry of TCRβ$^+$ mMR1:5-OP-RU$^+$ MAIT cells. *Right*: Cultured MAIT cells were re-stimulated briefly with PMA and Ionomycin before intracellular were measured. Representative of 2 experiments. (F) (*top*) Number of MAIT cells in the indicated chimeric mice. Donor BM cells were from *Mr1*$^{+/+}$ mice (black symbols) or *Mr1*$^{-/-}$ mice (red symbols); recipients were *Mr1*$^{+/+}$ (filled circles) or *Mr1*$^{-/-}$ mice (open circles). Thymus tissues were harvested after 8 weeks and analyzed by flow cytometry for MR1-tetramer binding cells. (*bottom*) Expression of CD44 and CD62L on MR1 tetramer-binding spleen cells from chimeric mice. Absolute numbers of CD62L$^+$ and CD62L$^-$ tetramer-binding spleen cells are shown.

Data analyzed by Kruskal-Wallis with Tukey post-test for multiple comparisons, displayed as mean ± SEM, NS: $P \geq 0.05$.

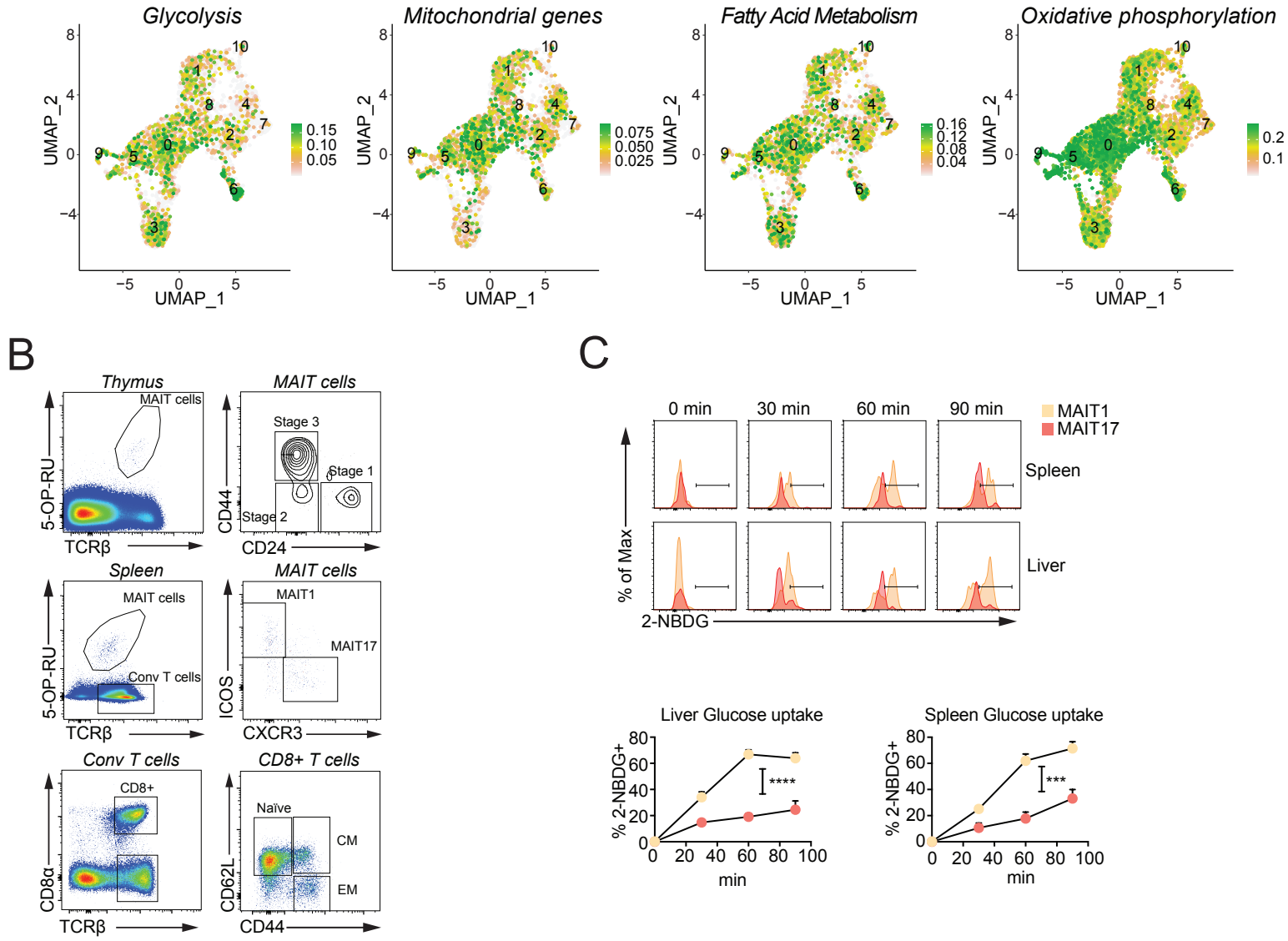
A
Glycolysis
Mitochondrial genes
Fatty Acid Metabolism
Oxidative phosphorylation
UMAP_1
UMAP_2
B
Thymus
MAIT cells
5-OP-RU
TCRβ
Stage 3
Stage 1
Stage 2
CD44
CD24
Spleen
Conv T cells
MAIT1
MAIT17
ICOS
CXCR3
Conv T cells
CD8+
CD8α
CD8+ T cells
Naïve
CM
EM
CD62L
C
0 min
30 min
60 min
90 min
MAIT1
MAIT17
Spleen
Liver
% of Max
2-NBDG
Liver Glucose uptake
Spleen Glucose uptake
% 2-NBDG+
min
****
***

Figure S4: Different metabolic signatures of mouse MAIT cell subsets

(A) UMAP of scRNA-seq data showing oxidative phosphorylation, mitochondrial gene, fatty acid metabolism and glycolysis signature scores for MAIT cells combined from thymus, spleen, liver and lung. (B) Gating strategy for subsets of mouse thymic (*top*) MAIT cells, splenic MAIT cells (*middle*) and conventional (conv) $CD8^+$ T cells (*bottom*). Spleen $TCR\beta^+$ $CD8\alpha^+$ T cells, excluding MAIT cells, were subdivided into naïve, central memory (CM) and effector memory (EM) subsets based on expression of CD62L and CD44. (C) MAIT cells were isolated from indicated tissues and kinetics of fluorescent glucose analog (2-NBDG) uptake in $CXCR3^+$ (MAIT1, yellow) and $ICOS^+$ (MAIT17, red) cell subsets were quantified; representative histograms of either Spleen (*top*) or Liver (*bottom*) MAIT cells for 2-NBDG uptake and dynamic quantification for both tissues (*bottom-left*, Liver; *bottom-right*, Spleen). Timepoints represent technical replicates from 8 pooled mice. Data analyzed by 2-way ANOVA with Geisser-Greenhouse correction, displayed as mean ± SEM, ***P<0.001 and ****P<0.0001.

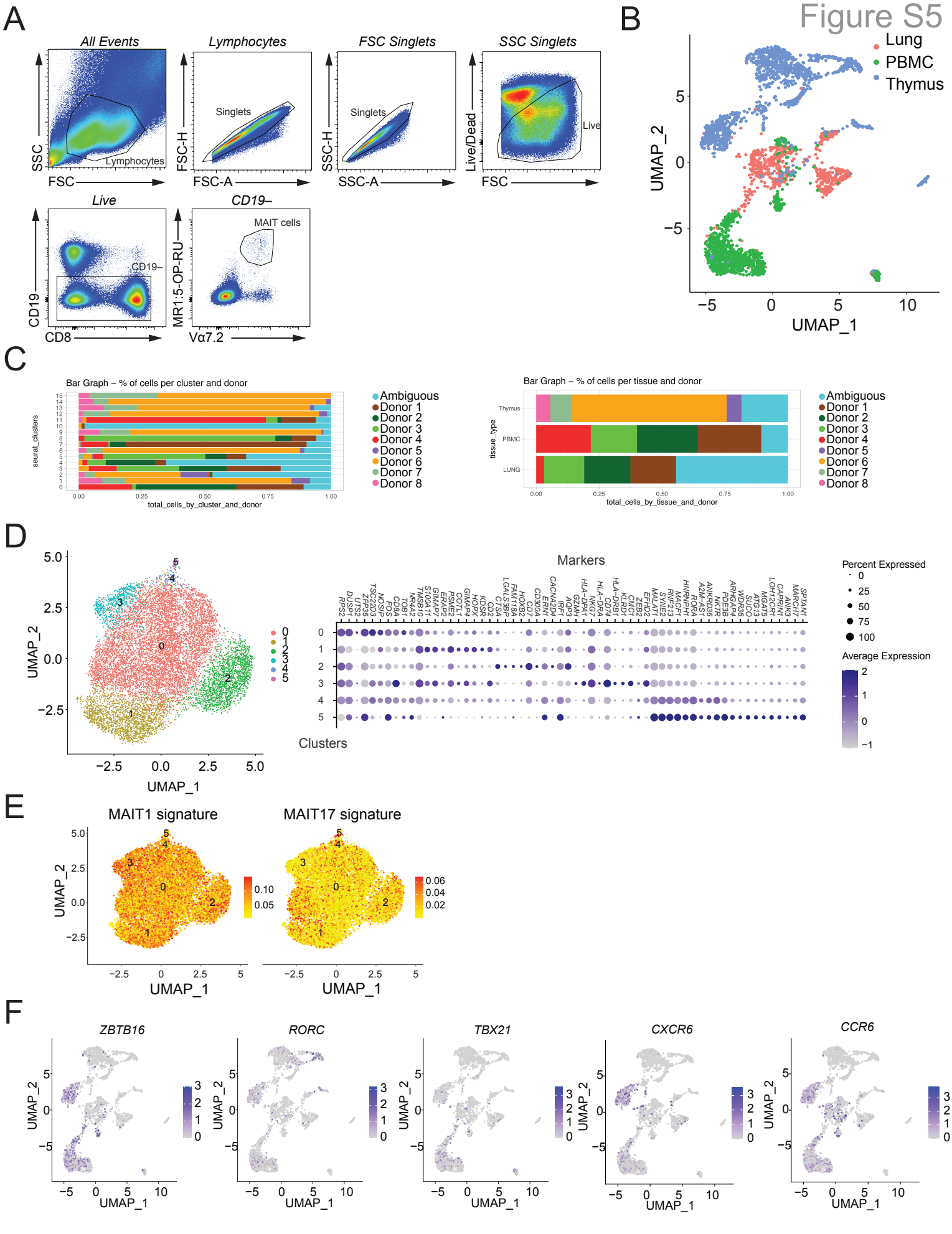
A
All Events
Lymphocytes
FSC Singlets
SSC Singlets
SSC
FSC
Lymphocytes
FSC-H
FSC-A
Singlets
SSC-H
SSC-A
Singlets
Live/Dead
FSC
Live
Live
CD19–
CD19
CD8
MR1:5-OP-RU
Vα7.2
MAIT cells
B
Lung
PBMC
Thymus
UMAP_2
UMAP_1
C
Bar Graph – % of cells per cluster and donor
seurat_clusters
total_cells_by_cluster_and_donor
Ambiguous
Donor 1
Donor 2
Donor 3
Donor 4
Donor 5
Donor 6
Donor 7
Donor 8
Bar Graph – % of cells per tissue and donor
tissue_type
Thymus
PBMC
LUNG
total_cells_by_tissue_and_donor
D
UMAP_2
UMAP_1
Markers
Clusters
Percent Expressed
Average Expression
E
MAIT1 signature
MAIT17 signature
UMAP_2
UMAP_1
F
ZBTB16
RORC
TBX21
CXCR6
CCR6
UMAP_2
UMAP_1

Figure S5: Human tissues have a distinct transcriptional signatures

(A) Representative flow cytometry gating to identify human MAIT cells in different tissues. Live/Dead Yellow negative single cell events were gated by excluding B cells ($CD19^+$). MAIT cells were identified as $V\alpha7.2$ TCR^+ and 5-OP-RU human MR1 $tetramer^+$ cells. (B) UMAP plots representing human MAIT cells colored by their origin from different tissues. (C) Bar graph indicating percentage of contributed by individual donors to the different MAIT cell clusters (*left*) and to MAIT cells in the different tissues (*right*). (D) Transcriptomic analysis of human MAIT cells from PMBCs from normal healthy donors. (*right*) UMAP plots were generated by combining cells from six individuals; (*left*) Dot plot showing top 5 positive marker genes in each cluster. (E) Score of MAIT1 or MAIT17 gene signatures from human PBMCs from normal donors. (F) UMAP plot of expression of *ZBTB16, RORC TBX21, CXCR6 and CCR6* by human MAIT cells combined from the different tissues.

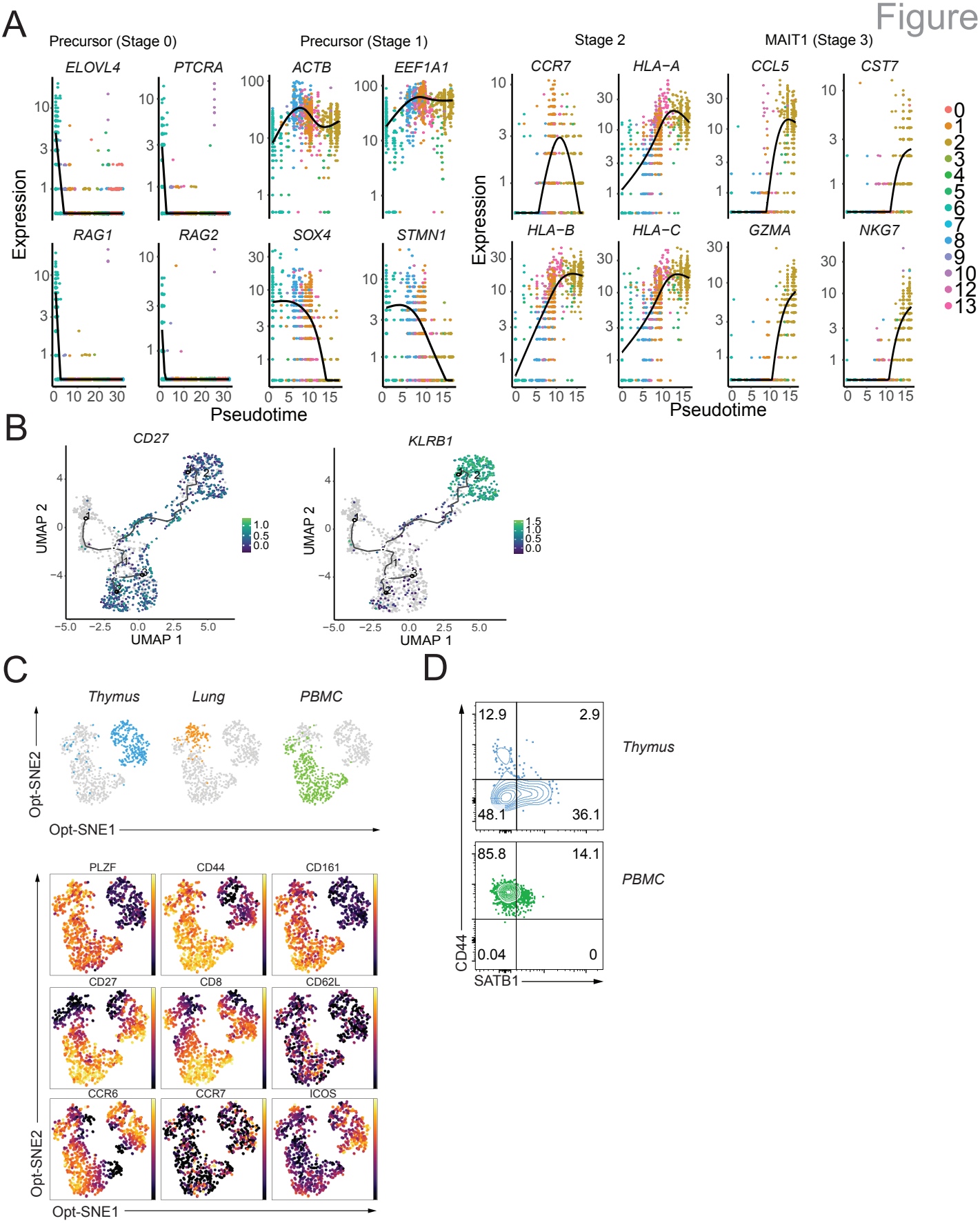
A
Precursor (Stage 0)
Precursor (Stage 1)
Stage 2
MAIT1 (Stage 3)
ELOVL4
PTCRA
ACTB
EEF1A1
CCR7
HLA-A
CCL5
CST7
RAG1
RAG2
SOX4
STMN1
HLA-B
HLA-C
GZMA
NKG7
Expression
Pseudotime
0
1
2
3
4
5
6
7
8
9
10
12
13
B
CD27
KLRB1
UMAP 2
UMAP 1
C
Thymus
Lung
PBMC
Opt-SNE2
Opt-SNE1
PLZF
CD44
CD161
CD27
CD8
CD62L
CCR6
CCR7
ICOS
D
12.9
2.9
48.1
36.1
Thymus
85.8
14.1
0.04
0
PBMC
CD44
SATB1

Figure S6: Transcriptional signatures reflected different stages of MAIT cell development in human thymus

(A) Expression of the indicated stage-specific genes along the pseudotime trajectory as constructed by Monocle 3. (B) Expression of *CD27* and *KLRB1* by MAIT cells from human thymus with a Monocle 3 trajectory analysis. (C) Human thymus, lung and blood tissue were processed for flow cytometry analysis. Human MAIT cells were detected as Vα7.2+ hMR1:5-OP-RU+ cells, as in Fig. S5A. Dimensional reduction was performed using Opt-SNE algorithm using the OMIQ software, considering either surface makers candidates or characteristics transcription factors identified by single cell RNA-seq. Representative of 2 experiments. (D) Expression of SATB1 and CD44 by human thymic MAIT cells (*top*) and MAIT cells in PMBCs (*bottom*). Representative of 2 experiments.

A

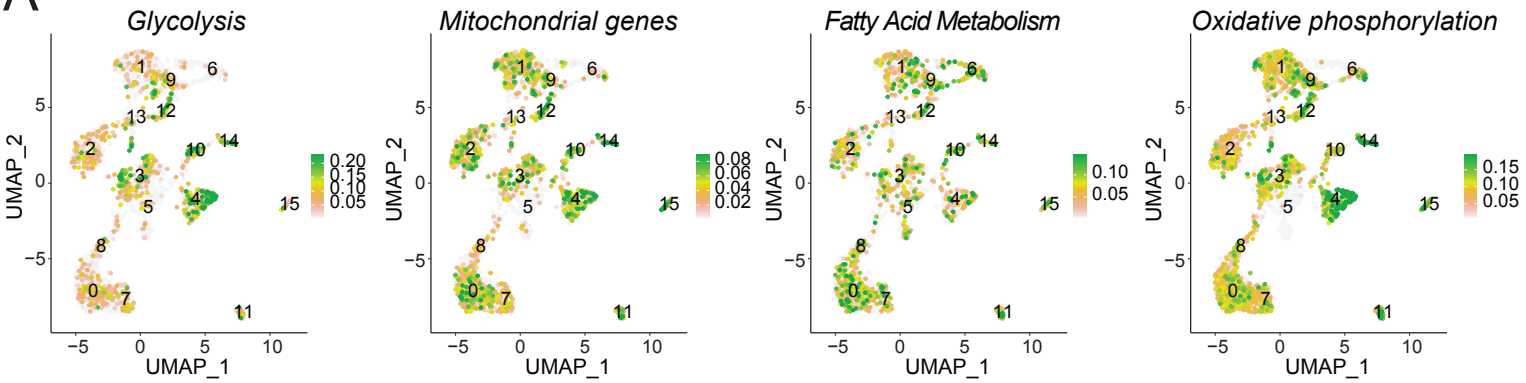
Glycolysis
Mitochondrial genes
Fatty Acid Metabolism
Oxidative phosphorylation
UMAP_1
UMAP_2

B

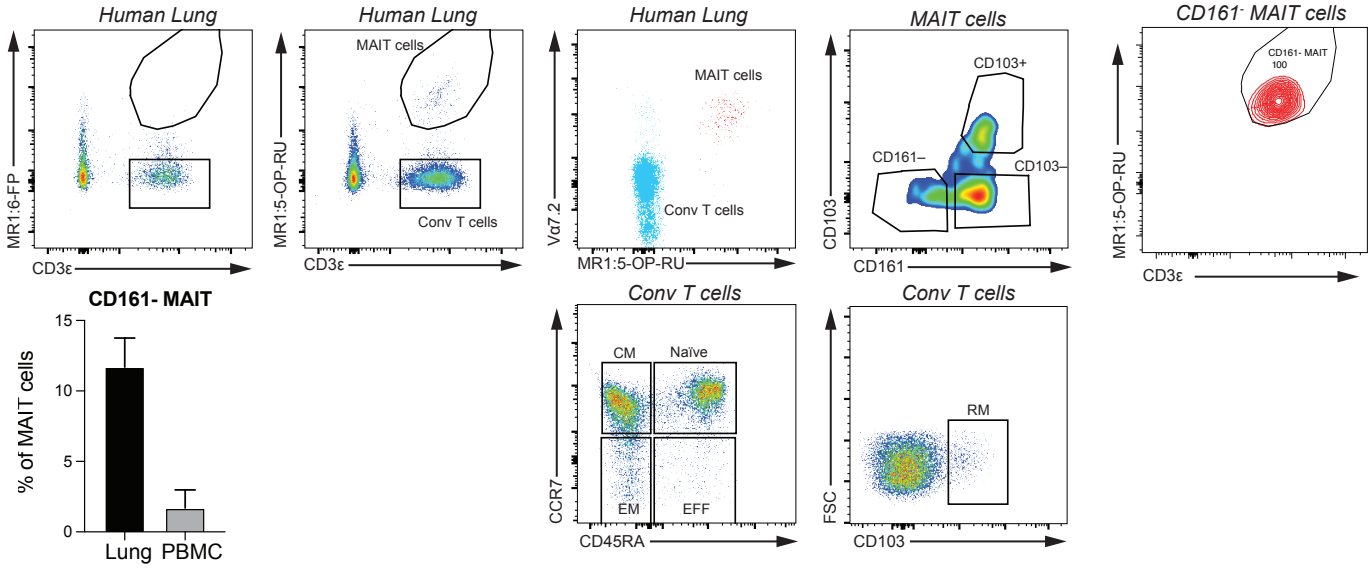
Human Lung
MAIT cells
Conv T cells
MAIT cells
CD161- MAIT cells
CD161- MAIT
100
CD103+
CD161–
CD103–
CD161- MAIT
% of MAIT cells
Lung
PBMC
Conv T cells
CM
Naïve
EM
EFF
RM
MR1:6-FP
MR1:5-OP-RU
CD3ε
Vα7.2
CD103
CD161
CCR7
CD45RA
FSC

Figure S7: Metabolic signature of human MAIT cells.

(A) UMAP showing the oxidative phosphorylation, mitochondrial genes, fatty acid metabolism and glycolysis signature scores for human MAIT cells combined form the four tissues. (B) Cells were isolated from human lung biopsies and stained with non-specific tetramer control MR1 loaded with 6FP (*left*) or 5-OP-RU loaded MR1 tetramer to identify MAIT cells (*right*). $CD3^+$ 5-OP-RU-$tetramer^+$ MAIT cells were further tested for Vα7.2 TCR and subdivided into three subsets based on expression of CD161 and CD103, as shown. TCRβ^+ $CD8^+$ T cells excluding MAIT cells were subdivided into naïve, central memory (CM), effector memory (EM) and resident memory (RM) subsets based on expression of CD45RA, CCR7 and CD103. On right, percentage of $CD161^-$ cells are shown in lung and PBMCs.

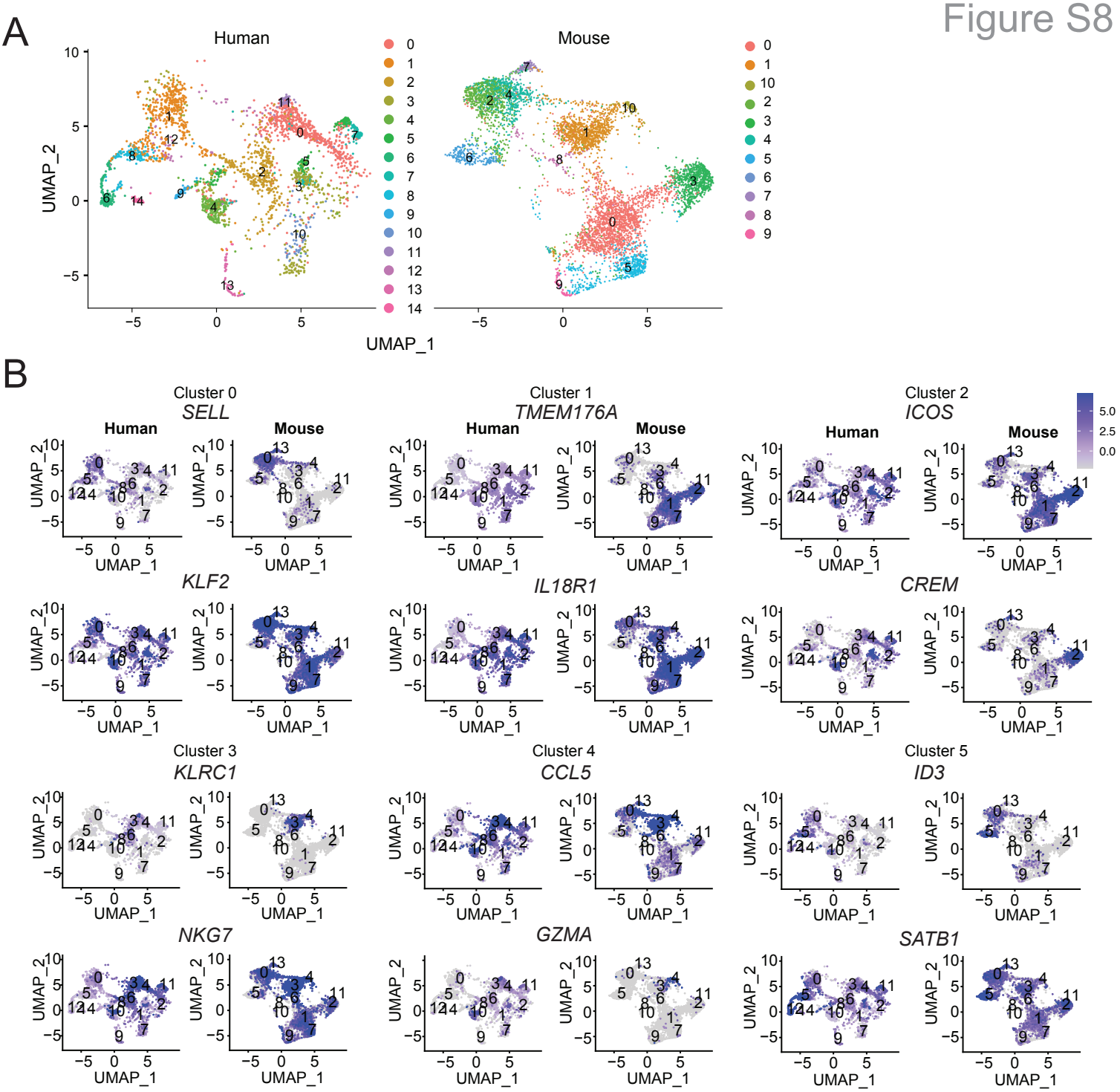
A
Human
Mouse
UMAP_2
UMAP_1
B
Cluster 0
SELL
Cluster 1
TMEM176A
Cluster 2
ICOS
KLF2
IL18R1
CREM
Cluster 3
KLRC1
Cluster 4
CCL5
Cluster 5
ID3
NKG7
GZMA
SATB1
Human
Mouse
5.0
2.5
0.0

Figure S8: Integration of human and mouse MAIT cell datasets.

(A) Integrated UMAP of mouse and human MAIT cells showing clusters of cells with same coordinates as in the Fig 7A. Cells are labeled according to the cluster numbers in Fig 5 A (human) and Fig 1A (mouse). (B) UMAPs showing expression by human and mouse MAIT cells of the top two marker genes of the indicated *i*-clusters.

Figure S9

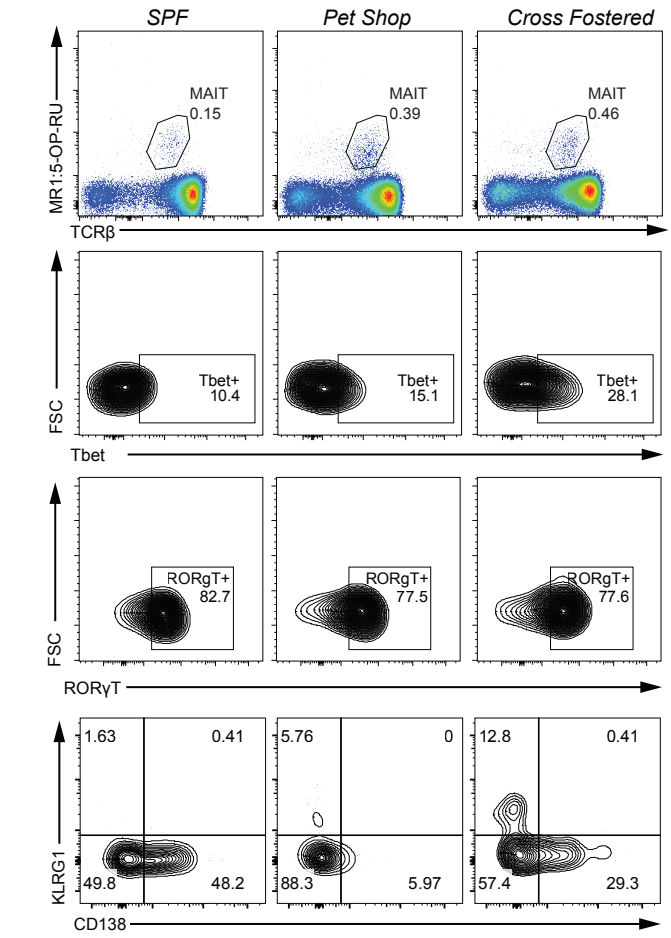
A
SPF
Pet Shop
Cross Fostered
MR1:5-OP-RU
TCRβ
MAIT
0.15
MAIT
0.39
MAIT
0.46
FSC
Tbet
Tbet+
10.4
Tbet+
15.1
Tbet+
28.1
FSC
RORγT
RORgT+
82.7
RORgT+
77.5
RORgT+
77.6
KLRG1
CD138
1.63
0.41
49.8
48.2
5.76
0
88.3
5.97
12.8
0.41
57.4
29.3

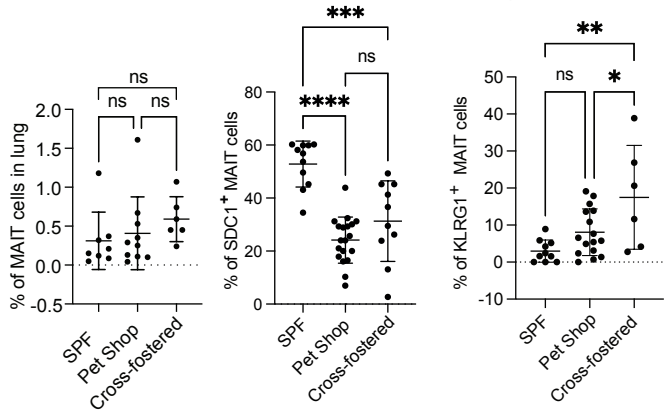
B
% of MAIT cells in lung
ns
ns
ns
SPF
Pet Shop
Cross-fostered
% of SDC1+ MAIT cells
***
ns
****
% of KLRG1+ MAIT cells
**
ns
*

Figure S9: Altered MAIT cell phenotype in pet shop and cross-fostered mice.

(A) Representative flow cytometry plots from SPF, pet store and cross-fostered mice showing percentage of lung MAIT cells, and the percentage of MAIT cells that expressed the indicated proteins. (B) Cumulative data of lung MAIT cell protein expression analyzed by one-way ANOVA with Tukey test displayed as mean± S.D. SPF mice n = 8, Pet shop mice n=10 and cross fostered mice n=6.

A

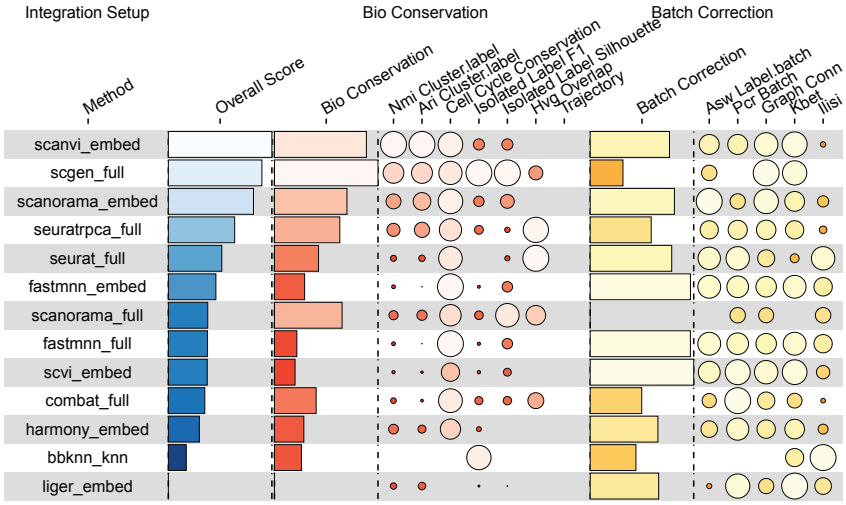
Integration Setup
Bio Conservation
Batch Correction
Method
Overall Score
Bio Conservation
Nmi Cluster.label
Ari Cluster.label
Cell Cycle Conservation
Isolated Label F1
Isolated Label Silhouette
Hvg Overlap
Trajectory
Batch Correction
Asw Label.batch
Pcr Batch
Graph Conn
Kbet
Ilisi
scanvi_embed
scgen_full
scanorama_embed
seuratrpca_full
seurat_full
fastmnn_embed
scanorama_full
fastmnn_full
scvi_embed
combat_full
harmony_embed
bbknn_knn
liger_embed

B

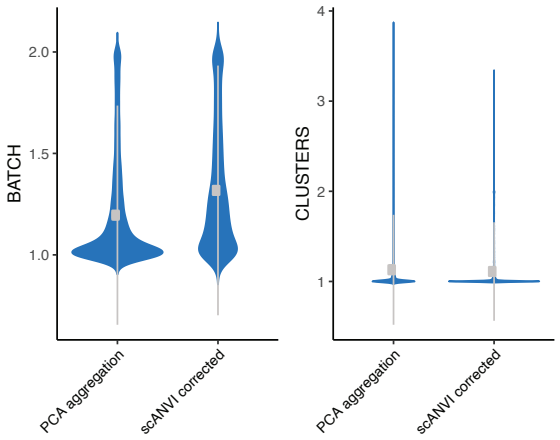
BATCH
CLUSTERS
PCA aggregation
scANVI corrected
PCA aggregation
scANVI corrected

C

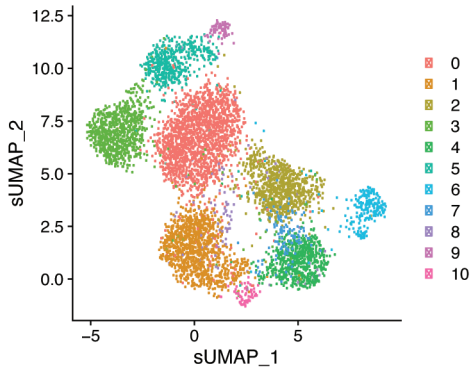
sUMAP_2
sUMAP_1
0
1
2
3
4
5
6
7
8
9
10

D

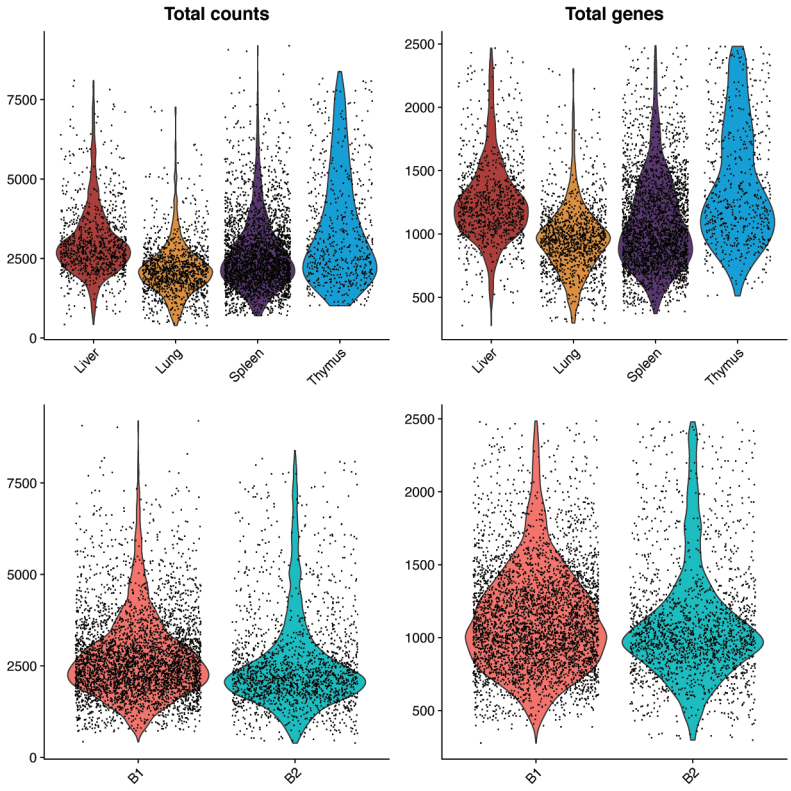
Total counts
Total genes
Liver
Lung
Spleen
Thymus
B1
B2

Figure S10: Batch effect correction and quality control of single cell libraries.

(A) Comparison of the performance of difference batch-effect correction methods. Performance metrics for conservation of biological changes and batch correction are indicated, as described (*70*). Overall scores are computed by a 40:60 weighted mean of these category scores, as described (*70*). scANVI method displayed best overall performance for our dataset. Color density indicates the ranking of the method, size of the circles the performance score. (B) Comparison of label conservation metrics obtained without (PCA-based aggregation shown in **Fig. 1A**) and with scANVI batch-effect correction. The distribution of local inverse Simpson's index (LISI) scores for the number of batches (*left*) and clusters (*right*). If major batch effect were present, then scANVI corrected LISI scores will show major differences from those obtained without correction. (C) Single-cell transcriptomes of mouse MAIT cells displayed by UMAP based on Seurat-based clustering of scANVI batch-effect corrected data displayed in **Fig. 1A** (without batch-effect correction). The color of the cells (dots) in the plot indicate their cluster annotations obtained without batch-effect correction. Cells from the original clusters also map onto distinct clusters in the batch-effect corrected clustering shown here. (D) Quality controls metrices of single-cell libraries from different organ and batches. Violin plots show the distribution of total UMI counts (*left*) and number of genes expressed in single cells (*right*) for the indicate batches and organs.